Bulgarian Chemical Communications, Volume 53, Issue 3 (pp. 327 - 342) 2021 *DOI: 10.34049/bcc.53.3.5375*

Geometrical optimization, PASS prediction, molecular docking, and *in silico* ADMET studies of thymidine derivatives against FimH adhesin of *Escherichia coli*

M. Anowar Hosen[1], A. Alam[1], M. Islam[1], Y. Fujii[2], Y. Ozeki[3], S. M. Abe Kawsar[1*]

[1] *Department of Chemistry, Faculty of Science, University of Chittagong, Chittagong-4331, Bangladesh*
[2] *School of Pharmaceutical Sciences, Nagasaki International University, 2825-7, Huis Ten Bosch-cho, Sasebo, Nagasaki 859-3298, Japan*
[3] *School of Sciences, Yokohama City University, 22-2, Seto, Kanazawa-ku, Yokohama 236-0027, Japan*

Received: January 22, 2021; Revised: July 28, 2021

Thymidine-containing derivatives are some of the most exigent analogs of drug molecules. In this investigation, several 5′-*O*-acyl thymidine derivatives (2–11) having different aliphatic and aromatic groups were employed for optimization, molecular docking, biological prediction, and physicochemical studies. Density functional theory (DFT) with B3LYP/3-21G was employed to demonstrate their thermochemical, atomic partial charge (APC), and molecular electrostatic potential (MEP) properties. Prediction of activity spectra for substances (PASS) revealed promising antibacterial, antiviral, and anti-carcinogenic activities of these thymidine derivatives compared to their antifungal activities. In support of this observation, their cytotoxic prediction and molecular docking studies were performed against FimH adhesin of *Escherichia coli* (PDB: 1TR7). The molecular docking studies exhibited that most of the molecules could bind to the near crucial catalytic binding site, Tyr48, Ile13, Ile52, Phe1, and Tyr137 of the lectin adhesin FimH, and the molecules were surrounded by other active site residues like Gln133, Asp47, Asn46, Asp54, Asn135, Asp140, and Ala6. Besides, these partially acylated thymidine derivatives were analyzed for their pharmacokinetic properties which revealed that the combination of *in silico* ADMET prediction and drug-likeness showed a promising pharmacokinetic profile. Overall, the present study might be useful for the development of thymidine-based potential antimicrobial drugs.

Keywords: Thymidine; adhesin FimH; MEP; PASS; ADMET; DFT

Abbreviations: DFT: density functional theory; ADMET: absorption, distribution, metabolism, elimination, toxicity, QM: quantum mechanical; LYP: Lee, Yang and Parr's; MEP: molecular electrostatic potential; PASS: prediction of activity spectra for substances.

INTRODUCTION

Nucleoside antibiotics have been under investigation for many years [1]. Some of the most clinically effective antiviral agents currently in use are purine or pyrimidine nucleoside analogs [2]. Thymidine, structurally known as deoxythymidine (Figure 1) is a pyrimidine-based nucleoside that constitutes a major part of one of the four nucleosides in DNA and is listed as a chemical teratogen [3]. Modification of hydroxyl (-OH) group at 3′ and 5′ position improves the antimicrobial activity of thymidine derivatives and brings about some potential antimicrobial agents [4-6]. As a result of screening synthetic compounds for potential antimicrobial activity, a study reported that azidothymidine (AZT) has potent bactericidal *in vitro* activity against various members of the family Enterobacteriaceae [7]. Azidothymidine (AZT) is one of the most popular thymidine derivatives (antiviral drug) in which 3′-hydroxyl (-OH) was modified by an azide group and is now used worldwide for the treatment of HIV infection [8]. AZT suppresses the mode of reverse transcription, a ticklish phase in the life cycle of a virus. Edoxudine is another thymidine-derived antiviral drug, strongly working against the herpes simplex virus [3]. Moreover, thymidine is used in cell biology to synchronize cells. Thymidine analog bromodeoxyuridine is often used for the detection of proliferating cells in living tissues. Thymidine is also catabolized to identify TP-expressing tumor xenografts [9]. Furthermore, after alteration of hydroxyl (-OH) group in nucleoside derivatives uridine and cytidine also have potential antimicrobial activity [10-17].

Antagonists of the *Escherichia coli* type-1 fimbrial adhesin FimH are recognized as attractive alternatives for antibiotic therapies and prophylaxes against acute and recurrent bacterial infections. Pyrimidine nucleosides are influential antimicrobial agents that act as a specific inhibitor of the dihydrofolate reductase of bacteria. Some recent computational studies reported that modified thymidine derivatives are also possessing significant thermodynamic stability and pharmacological properties [18]. Pathogenic *E. coli* adheres *via* the FimH adhesin at the tip of their

*To whom all correspondence should be sent:
E-mail: akawsarabe@yahoo.com

type-1 fimbriae to mannosylated glycan receptors on epithelial linings [19, 20]. The use of mannose-based anti-adhesives for the selective inhibition of type 1-pilus mediated bacterial adhesion has attracted great interest for the non-antibiotic treatment of urinary tract [19, 21] and intestinal [20, 22, 23] infections caused by pathogenic *E. coli*. These bacteria can express an arsenal of multiple adhesins, lectins with a variable immunoglobulin fold, for their attachment to and colonization of host cells.

Computational chemistry is a popular tool to predict the physicochemical, and biological properties of synthesized chemicals [24-28]. In this context, the potent antimicrobial efficacy of several thymidine derivatives 2–11 (Table 1) with various aliphatic and aromatic chains was investigated by molecular docking against lectin FimH of *Escherichia coli* (PDB: 1TR7) along with the prediction of activity spectra for substances (PASS). In addition, attempts were taken to optimize the acylated thymidine derivatives to predict their physicochemical and thermochemical behavior based on DFT (B3LYP/3-21G) approach with cytotoxicity. Finally, designed thymidine derivatives were analyzed for their pharmacokinetic properties which revealed that the combination of *in silico* ADMET prediction, and drug-likeness calculation gave a promising pharmacokinetic profile. Hence, this research work scintillates on the development of antimicrobial lead molecules from thymidine derivatives against lectin FimH *in silico* tools and studies their pharmacokinetic and toxicity properties.

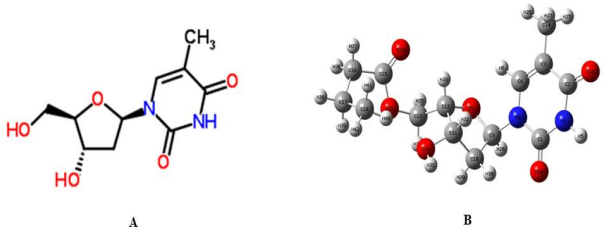

Figure 1. Chemical structure (**A**) and optimized molecular structure (**B**) of thymidine.

EXPERIMENTAL

Materials and methods

Molecular docking has become an increasingly important tool for drug discovery to predict drug interactions with receptor proteins. The blind docking method demonstrates a search throughout the whole surface of the protein molecule for binding sites. The following software was used in the present study: i) Gaussian 09, ii) AutoDock 4.2.6, iii) Swiss-Pdb 4.1.0, iv) Python 3.8.2, v) Discovery Studio 3.5, vi) PyMOL 2.3, and vii) LigPlot þ v.2.2.

Computational Details

Optimization of thymidine derivatives by DFT

In computational drug design study, quantum mechanical (QM) methods have gained attention on the calculation of thermodynamic properties, molecular orbital features, dipole moment, as well as interpretation of different types of interactions [29]. Molecular geometry optimization and further modification of all thymidine derivatives were carried out using the Gaussian 09 program [29]. Density functional theory (DFT) with Beck's (B) [30] three-parameter hybrid model, Lee, Yang, and Parr's (LYP) [31] correlation functional under 3-21G basis set was employed to optimize and predict their thermochemical properties. Molecular weight, heat capacity, entropy, free energy, atomic partial charge, and molecular electrostatic potential were calculated for all the derivatives.

PASS prediction

Web-based prediction of activity spectra for substances (PASS) (http://www.pharmaexpert.ru/PASSonline/index.php) was employed for the prediction of the biological spectrum of these thymidine esters [32]. Firstly, structures of the thymidine derivatives were drawn and converted into their smiles formats by using SwissADME free web tools (http://www.swissadme.ch), which were used to predict the biological spectrum using PASS online software. This program is designed to anticipate more than 4000 forms of biological activity including drug and non-drug actions and can be used to identify the most probable targets with 90% accuracy. PASS results are expressed as Pa (probability for active compound) and Pi (probability for inactive compound). Having probabilities, the Pa and Pi values vary from 0.000 to 1.000, and in general, $Pa + Pi \neq 1$, since these probabilities are calculated freely. The activities with $Pa > Pi$ are only considered as possible for a particular drug. The PASS prediction results were interpreted and used flexibly, *viz*. (i) when $Pa > 0.7$, the chance to find the activity experimentally is high, (ii) if $0.5 < Pa < 0.7$, the possibility to search the activity experimentally is low, but the compound is probably not so similar to known pharmaceutical agents, and (iii) if $Pa < 0.5$, the feasibility to find the activity experimentally is lower, but with a chance to find a structurally similar pharmaceutical agent. So, the prediction of

the activity of the spectrum of a drug is known as its intrinsic property.

Protein preparation and visualization

The 3D crystal structure of lectin FimH of *Escherichia coli* (PDB: 1TR7) was retrieved in pdb format from the protein data bank [33]. All hetero atoms and water molecules were removed using PyMol (version 1.3) software packages [34]. Swiss-Pdb viewer software (version 4.1.0) was employed for energy minimization of the protein [35]. Then optimized thymidine ligands were subjected to molecular docking study against *E. coli* (1TR7) (Figure 2). In fine, molecular docking simulation was rendered by PyRx software (version 0.8) [36] considering the protein as a macromolecule and the drug as a ligand. AutodockVina was employed for docking analysis, and AutoDock Tools (ADT) of the MGL software package was used to convert pdb into pdbqt format to input protein and ligands. The size of the grid box in AutoDockVina was kept at 46.9741, 34.6094, and 41.4160 Å for X, Y, Z directions, respectively. After the completion of docking, both the macromolecule and ligand structures were saved in pdbqt format needed by Accelrys Discovery Studio (version 4.1) to explore and visualize the docking result and search the nonbonding interactions between ligands and amino acid residues of receptor protein [37]. *In vitro*, FimH tends to form amyloid-like aggregates at pH 3, but neither at pH 5, nor 7. Since 1TR7 has its crystal structure in a state that represents the pharmacological target for the development of new drugs, it was selected for computational studies. The validation was checked by PROCHECK online server and it gave 98.08 overall quality factors in ERRAT (http://www.ncbi.nlm.nih.gov/entrez/query.fcgi?cmd=Retrieve&db=PubMed&list_uids=8401235&dopt=Abstract), 96.23% score in VERIFY 3D (https://www.ncbi.nlm.nih.gov/pubmed/1853201?dopt=Abstract). PDBsum online server was also used to check the validation of the main protease receptor with Ramachandran plot (Figure 3) which revealed that 88.07% residues were in the allowed region and no residues were missed.

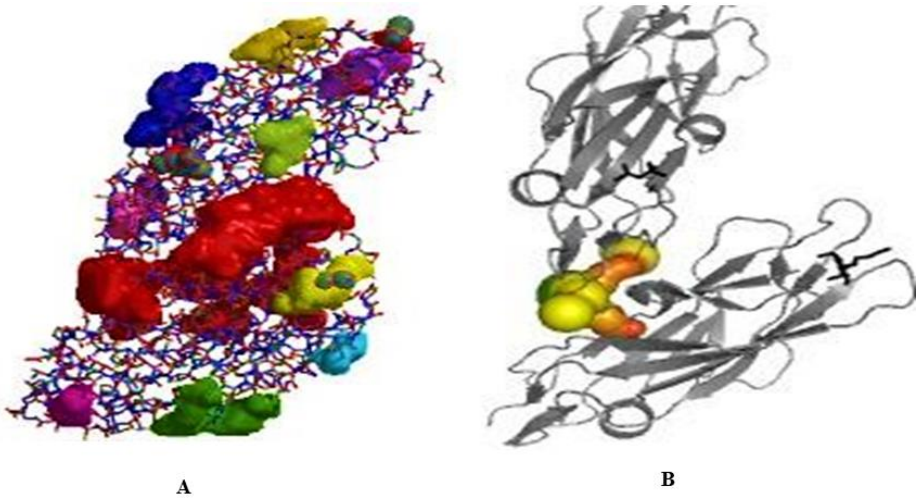

Figure 2. Binding pocket (A) and crystal structure (B) of 1TR7.

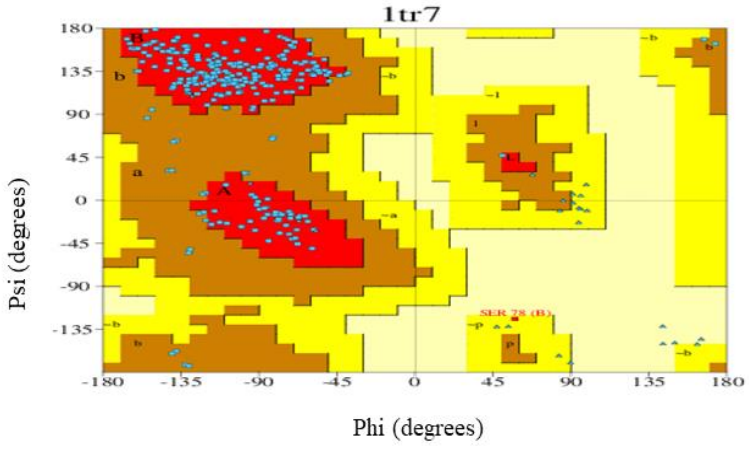

Figure 3. Ramachandran plot for lectin FimH 1TR7.

Docking validation protocol

The docking validation was performed by extracting the co-crystallized ligand (DEG - butyl α-D-mannopyranoside) of the lectin FimH (PDB: 1TR7) and re-docking it into the same position. The lowest energy pose obtained on re-docking and the co-crystallized ligands were superimposed using PyMOL 2.3, and its root means square deviation (RMSD) was calculated between these two superimposed ligands. To validate the docking process, the RMSD must be within a reliable range of 2 Å [38, 39]. It was done to enhance ligand enrichment, which is necessary to test the docking procedure.

In silico pharmacokinetics ADMET and drug-like parameters prediction

To point out potential drug molecules, the ADMET properties were determined for the preliminary prediction of the pharmacokinetic, physicochemical, and drug-like properties in the drug discovery process. *In silico* study suggests an indication to the accession of pharmacokinetic parameters (adsorption, distribution, metabolism, excretion, and toxicity, ADMET) [40], its absorption in the human intestine, percolation of the blood-brain barrier and the central nervous system. The metabolism indicates the chemical biotransformation of a drug by the body, total clearance of drugs and the toxicity levels of the molecules. The drug-likeliness of a molecule is expressed by Lipinski's rule of five parameters (molecular weight <500 Da, no more than 5 hydrogen bond donors, hydrogen bond acceptors should be less than 10 and log P should not be greater than 5). Lipinski's rule of five properties was obtained from the SwissADME server (www.swissadme.ch/index.php) [41]. Prediction of the drug-likeness of the designed thymidine derivatives was also assessed by rule-based filters from Lipinski, Ghose, Veber, and Egan, and the synthetic accessibility difficulty scale was 1–10.

RESULTS AND DISCUSSION

Designed and optimized thymidine derivatives

In the present study, ten thymidine derivatives were modified with different aliphatic and aromatic chains (2–11) (Table 1) and were subjected to a quantum chemical study to realize the mode of their thermochemical properties. Initially, partially acylated derivatives were predicted for biological activities using the PASS program. The observed activities were then rationalized by calculating their physicochemical (DFT method), cytotoxicity (predicted), molecular docking, and with the combination *in silico* ADMET and drug-likeness properties.

Table 1. List of thymidine derivatives 2-11.

Entry	Name of the compound	Acyl groups
1	Thymidine	--
2	5′-*O*-Propionylthymidine	CH_3CH_2CO-
3	5′-*O*-Butyrylthymidine	$CH_3(CH_2)_2CO$-
4	5′-*O*-Hexanoylthymidine	$CH_3(CH_2)_4CO$-
5	5′-*O*-Nonanoylthymidine	$CH_3(CH_2)_7CO$-
6	5′-*O*-Lauroylthymidine	$CH_3(CH_2)_{10}CO$-
7	5′-*O*-Palmitoylthymidine	$CH_3(CH_2)_{14}CO$-
8	5′-*O*-Stearoylthymidine	$CH_3(CH_2)_{16}CO$-
9	5′-*O*-4-Chlorobenzoylthymidine	4-Cl.C_6H_4CO-
10	5′-*O*-3-Bromobenzoylthymidine	3-Br.C_6H_4CO-
11	5′-*O*-Tritylthymidine	$(C_6H_5)_3C$-

Thermochemical study

The spontaneous reaction and stability of a product was elucidated from the free energy and enthalpy values [42]. Highly negative values were more significant for thermal stability. In a quantum chemical study, dipole moment influences non-bonded interactions of hydrogen bond formation smoothly. The binding property can also be improved by increasing of the dipole moment [43]. Free energy (G) is another important factor to display the interaction of binding partners, where a negative value is favorable for spontaneous binding and interaction. Greater negative values reveal better thermodynamic properties. Presences of a bulky acylating group suggesting the possible improvement of free energies are presented in Table 2. In this study, all thymidine derivatives possess a greater negative value for free energy than the parent thymidine, and hence, indicated that the insertion of the acyl group could improve interaction and binding of these molecules with different microbial enzymes. Due to these higher values (–1670.229 to –3774.042 Hartree), halobenzoyl derivatives 9–11 exhibited a better score against *E. coli*. Furthermore, the increased negative values of derivatives 2–8 suggested that these derivatives were thermodynamically more stable.

Table 2. Stoichiometry, molecular weight, heat capacity, entropy, and total free energy of thymidine derivatives.

Entry	Stoichiometry	Formula weight (g/mol)	Heat capacity (cal/mol-kelvin)	Entropy (cal/mol-kelvin)	Total free energy (Hartree)
1	$C_{10}H_{14}N_2O_5$	242.230	59.701	125.981	-870.318
2	$C_{13}H_{18}N_2O_6$	298.291	74.723	144.447	-1061.254
3	$C_{14}H_{20}N_2O_6$	312.120	80.664	156.868	-1100.352
4	$C_{16}H_{24}N_2O_6$	340.371	90.173	169.613	-1178.554
5	$C_{19}H_{30}N_2O_6$	382.451	104.181	182.114	-1295.853
6	$C_{22}H_{36}N_2O_6$	424.530	118.450	213.440	-1413.161
7	$C_{26}H_{44}N_2O_6$	480.585	136.963	240.043	-1569.554
8	$C_{28}H_{48}N_2O_6$	508.693	146.185	246.456	-1647.774
9	$C_{17}H_{17}N_2O_6Cl$	380.780	88.157	168.941	-1670.229
10	$C_{17}H_{17}N_2O_6Br$	425.231	87.893	171.081	-3774.042
11	$C_{29}H_{28}N_2O_5$	484.540	119.760	200.099	-1598.771

Table 3. Predicted biological activities of the thymidine derivatives using PASS software.

Entry	Biological activity							
	Antibacterial		Antifungal		Antiviral		Anti-carcinogenic	
	Pa	Pi	Pa	Pi	Pa	Pi	Pa	Pi
1	0.432	0.024	0.240	0.112	0.806	0.004	0.806	0.005
2	0.463	0.078	0.292	0.084	0.744	0.004	0.797	0.005
3	0.413	0.027	0.300	0.081	0.737	0.004	0.829	0.004
4	0.515	0.027	0.319	0.074	0.724	0.004	0.830	0.004
5	0.515	0.027	0.319	0.074	0.724	0.004	0.830	0.004
6	0.515	0.027	0.319	0.074	0.724	0.004	0.830	0.004
7	0.515	0.027	0.319	0.074	0.724	0.004	0.830	0.004
8	0.515	0.027	0.319	0.074	0.724	0.004	0.830	0.004
9	0.360	0.040	0.258	0.102	0.657	0.005	0.622	0.012
10	0.385	0.034	0.262	0.100	0.648	0.005	0.510	0.018
11	0.348	0.084	0.762	0.011	0.776	0.004	0.659	0.010

Another remarkable change observed was that with the increase of molecular weight, heat capacity, entropy, and free energy sharply increased for compounds 2 to 8 which have a long acyl chain. But fluctuations were found for the aromatic ring-containing derivatives 9–11. In fine, all of these properties may contribute to show higher chemical activity in the drug-related chemical and biochemical fields.

Computational evaluation of antimicrobial activities: PASS

The PASS results were designated as Pa and Pi which are presented in Table 3. It was manifest from prediction Table 3, that thymidine derivatives 2–11 showed $0.34 < Pa < 0.51$ for antibacterial, $0.29 < Pa < 0.76$ for antifungal, $0.64 < Pa < 0.80$ for antiviral and $0.51 < Pa < 0.83$ for anti-carcinogenic activity. This expressly revealed that these molecules were more prone to viruses and bacteria as compared to fungal pathogens. However, attachment of additional aliphatic acyl chains (C-2 to C-18, compounds 2–8) increased the antibacterial activity (Pa ¼ 0.515) compared to thymidine (1, Pa ¼ 0.432), whereas attachment of chloro- and bromo-substituted benzoyl groups did not lead to reasonable improvement (derivatives 9–11). The same scenario was observed for the antiviral activity where acyl chain derivatives 2–8 revealed improved values than the halo-benzoyl derivatives 9 and 10. But compound 11 which has the tri-phenyl group exhibited the highest antiviral activity (Pa ¼ 0.776). We have also predicted the anti-carcinogenic property of these derivatives. Thus, PASS predication exhibited $0.51 < Pa < 0.83$ for anti-carcinogenic activity which indicated that the thymidine derivatives were more potent as anti-carcinogenic agents than previous antimicrobial agents. Significantly, antibacterial, antiviral, and anti-carcinogenic properties of thymidine derivatives with saturated acyl chains (2–8) were found to be more promising than those of halobenzoyl and tri-phenyl derivatives (9–11) [44].

Atomic partial charge

The polarity of chemical bonds often indicates the structures and reactivity [45]. The dipole moment is just a vector, but it does not give the polarity of the molecule. Several methods have been suggested for assigning partial charges to the atoms of a molecule, including both quantum chemical and empirical schemes. Two different methods (Mulliken and NBO) have been utilized to

compute the partial charges of all drug atoms including both quantum chemical and empirical schemes [46]. They are the most recognized population analysis methods and have a significant contribution to the application of quantum chemical calculations to a molecular system because dipole moment and molecular polarizability are also related to atomic charges [47]. Here, all the hydrogen atoms showed a positive charge in both methods, and other electronegative atoms (N and O) negative charge in both methods as expected (Figure 4).

Derivative 6, (C-1 and C-15) showed a greater positive charge due to the presence of highly electronegative oxygen (O-27, O-29, and O-31), nitrogen (N-7) atoms, and H-5 exhibited a higher positive value than another hydrogen because of the oxygen atom of the hydroxyl (-OH) group. Similarly, derivatives **7** (C-1, C-25, and C-40), 8 (C-1, C-24 and, C-36), and 9, 10 (C-6 and C-13) displayed a positive charge in both methods due to the presence of oxygen atom of the carbonyl group and halogen atom (Br) in the aromatic ring.

Molecular electrostatic potential (MEP)

Molecular electrostatic potential (MEP) is globally preferred as a map of reactivity that reveals the most suitable region for organic molecules to perform electrophilic and nucleophilic reactions of charged point-like reagents [48]. It helps to explore the biological recognition process and hydrogen bonding interaction [49]. MEP counter map provides a simple way to predict how different geometry could interact. The MEP of the title compound was obtained based on the B3LYP with basis set 3-21G optimized result and is shown in Figure 5. The MEP is very useful in the study of molecular structure with physicochemical features relationship [50]. MEP was calculated to determine the reactive sites for electrophilic and nucleophilic attacks of the optimized structure of thymidine 1 and its derivatives 2, 4, and 7. The different colors of the electrostatic potential indicate different values. The potentiality of the attacking zone decreases in the sequence: blue > green > yellow > orange > red. The maximum negative area is displayed by red color where electrophiles can easily attack and the maximum positive area is indicated by blue color which is suitable for nucleophilic attack. Moreover, the green color showed zero potential zones.

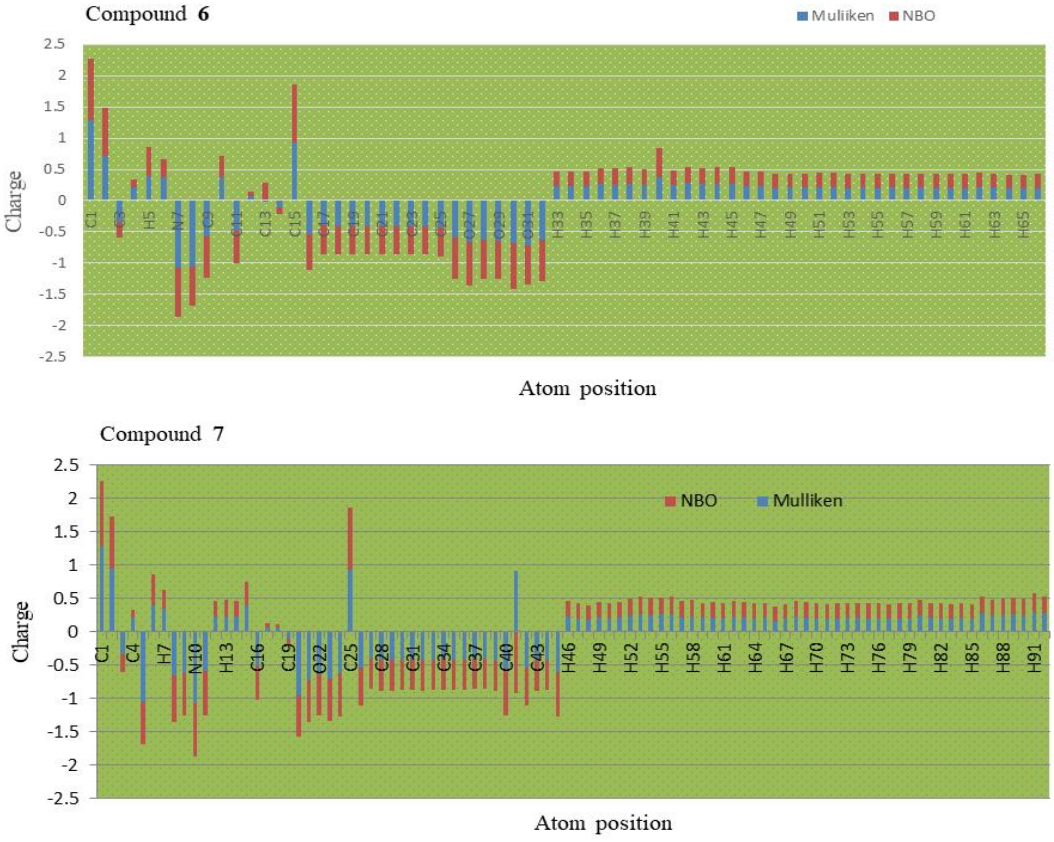

Figure 4. Atomic partial charges of compounds 6 and 7.

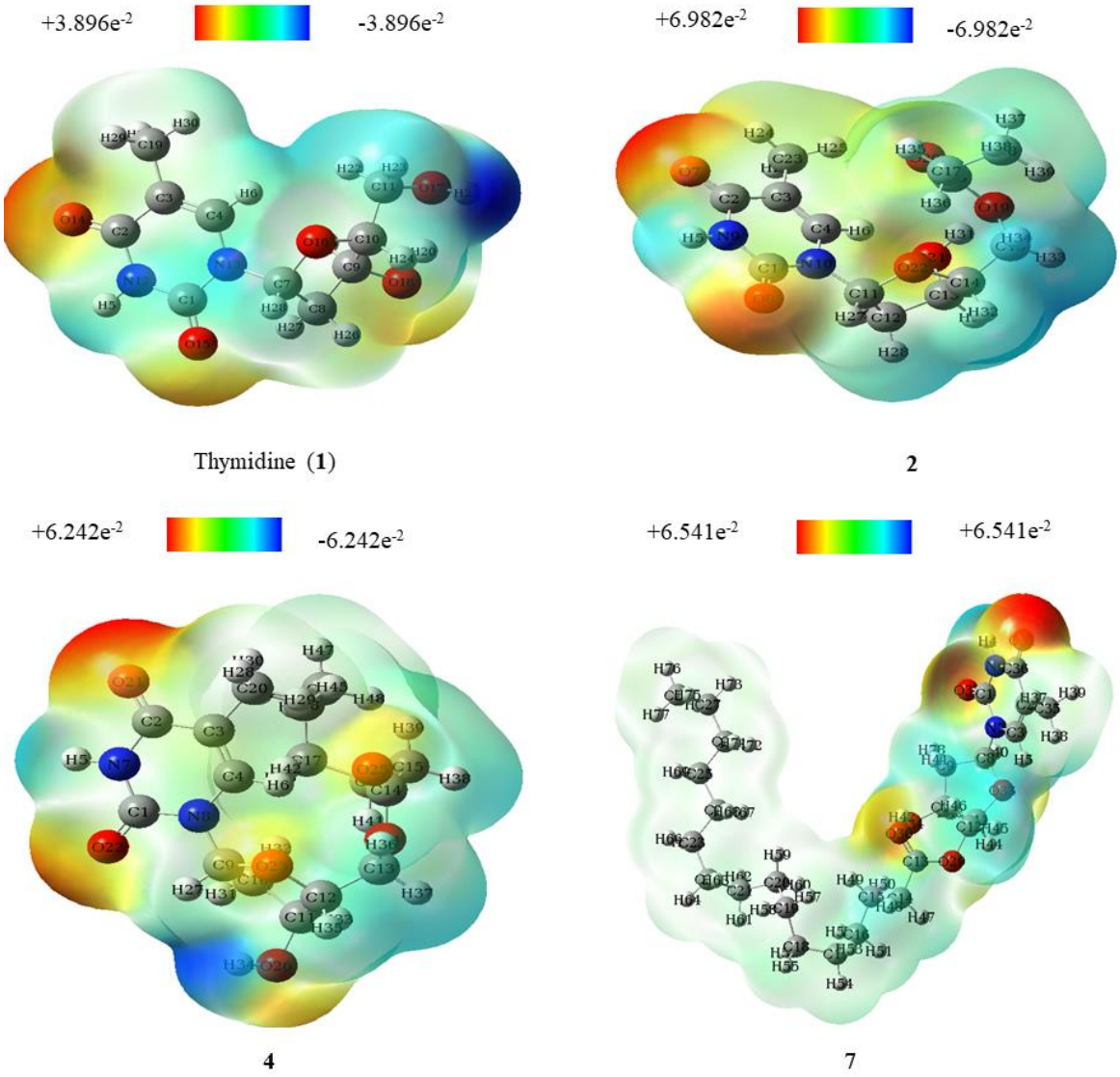

Figure 5. Molecular electrostatic potential map of thymidine and its derivatives **2**, **4**, and **7**.

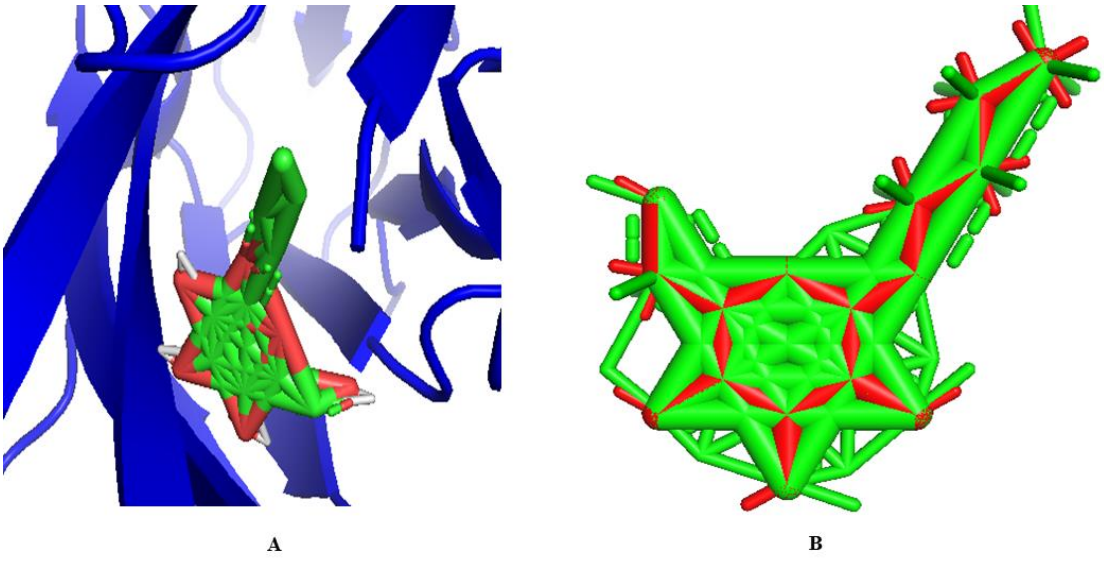

Figure 6. Re-docking pose with the RMSD value of 0.402 Å (red = original, green = docked).

Docking validation study

To identify the ability of docking algorithms to determine the conformation of the protein-bound ligand, re-docking of the co-crystallized ligand was employed to validate the accuracy of the docking procedure. Figure 6 indicates the superimposed view between the docked ligand conformation and the co-crystallized ligand conformation and the RMSD value is 0.402 Å. The complex was found to interact with the same amino acid residues compared to those reported in the present study. The bulky symmetric molecules could be exchanged in the binding site during docking, as is the case in this investigation; the RMSD would be at a very high level. On the contrary, the small compounds could gain low RMSD easily even when placed randomly. Some reported studies [51-53] have suggested a new benchmark for the quality of docking poses based on visual inspection. For visual inspection, Figure 7 shows the 2D visualization of the interactions between a generated docking pose and the experimental ligand conformation. The results of this visual inspection showed the same interactions as in the experimental binding mode, as observed in Figure 7. This result revealed that only visual inspection is not a reliable parameter for the quality of docking poses for docking validation, and the use of visual inspection as a new reference is essential. These partially proved the efficacy and validity of the docking protocol.

Molecular docking studies

Estimation of the feasible binding geometries and interactions between ligand and the active site of proteins was obtained from molecular docking [54]. All selected molecules were subjected to docking into the same binding pocket of lectin FimH of *E. coli* (PDB: 1TR7) using similar optimized docking conditions to identify their binding mode. The results of the docking exploration showed that all thymidine derivatives, along with the parent molecule, gain binding affinities ranging from -5.8 to -6.9 kcal/mol. As shown in Table 4, all the derivatives 2–11 showed comparatively higher binding affinities compared to the parent drug, thymidine 1. These results indicated that modification of the –OH group, along with an aromatic ring or an aliphatic chain molecule improved the binding affinity, while the insertion of halo-benzoyl groups like -Cl and -Br, made some fickleness in binding affinities. However, modification with halogenated aromatic rings increased the binding affinity. The docked pose showed that the drug molecules bind within the active site of the *E. coli* (1TR7) macromolecular structure (Figure 7). Figures 8 and 9 show that thymidine derivatives 9, 10, and 11 (binding affinities -6.7, -6.9, and -6.7 kcal/mol, respectively) bind firmly through hydrophobic bonds with the catalytic binding site Tyr48, Ile52, Ala6, and Ile13, where these residues exhibited alkyl, pi-alkyl pi-sigma and pi-pi stacked interaction. The pi-pi interaction revealed the tight binding with the active site. Besides, Gln133, Asn46, Asp47, Tyr137, and Phe1 which were the highly specific binding pocket of FimH were also found to form hydrogen and electrostatic bonds. It is evident from the structural contrast that compounds 9–11 have an additional aromatic (halogenated ring and tri-phenyl ring) substituent in the parent structure, indicating a high density of electrons in the molecule leading to a comparatively higher binding affinity (6.7 to -6.9 kcal/mol). On the other hand, thymidine derivatives 2, 3, and 4 revealed three similar binding pockets with tyrosine gate Tyr48, Asn46, Asp47, and Pro49 through both hydrogen and hydrophobic bonds. These ligands were bonded in a deep and polar pocket at the N-terminal end of FimH, in which the amino acids Asn46, Asp47, Gln41, and Asn135 create a dense network of nine hydrogen bonds with each hydroxyl group of the ribose ring. In addition, Asn46 showed a closer distance of 1.831 Å for derivative 4.

The derivatives 5–8, which were modified with a long aliphatic chain (nonanoyl, lauroyl, palmitoyl, and stearoyl), enhanced the binding affinities by specific recognition events at post-glycosidic linkage atomic positions two to three with Ile52 and Tyr48 of the tyrosine gate. Interestingly, these derivatives specifically bind through the hydrogen bond with the specific pocket Ile13, Ile52, Asn46, Asn135, Asp47, Asp54, and Gln133. Among all of these residues, Ile52 was found in a close interaction (1.770 Å). Besides, derivatives 9–11 (along with Phe1) displayed the maximum π-alkyl, π-cation, and π- π interactions with the Tyr48 Ile52 and Ile13 indicating a tight binding with the active site.

Table 4. Binding affinities and non-bonding interactions of thymidine and its derivatives.

Entry	Protein	Binding affinity (kcal/mol)	Bond category	Residues in contact	Interaction types	Distance (Å)
1	1TR7	-5.8	Hydrogen	ASN135	H	2.387
			Hydrogen	ASP140	H	2.549
			Hydrogen	THR53	C	3.417
			Hydrophobic	THR134	PS	3.621
2	1TR7	-6.0	Hydrogen	ASN135	H	2.168
			Hydrogen	ASP47	H	2.406
			Hydrogen	GLN41	H	2.911
			Hydrogen	TYR48	H	2.140
			Hydrophobic	ALA6	A	3.602
			Hydrophobic	ALA6	PA	5.462
3	1TR7	-6.1	Hydrogen	ASP47	H	2.336
			Hydrogen	TYR48	H	2.204
			Hydrophobic	PRO49	A	4.583
			Hydrophobic	PRO49	PA	4.863
			Hydrophobic	PRO104	PA	5.223
4	1TR7	-6.4	Hydrogen	ASP47	H	2.725
			Hydrogen	TYR48	H	2.920
			Hydrogen	ASN46	H	1.831
			Hydrophobic	LYS76	A	3.716
			Hydrophobic	PRO49	PA	4.858
5	1TR7	-6.5	Hydrogen	ILE52	H	1.951
			Hydrogen	ASN46	H	2.368
			Hydrogen	ASN46	H	2.447
			Hydrogen	ILE13	H	2.805
			Hydrogen	ASP54	H	1.898
			Hydrogen	GLN133	H	2.849
			Hydrogen	ASN135	H	2.431
			Hydrophobic	TYR48	PA	4.499
6	1TR7	-6.5	Hydrogen	ASP47	H	2.531
			Hydrogen	PRO49	H	4.926
			Hydrogen	SER39	H	2.914
			Hydrophobic	ASN46	PS	3.970
			Hydrophobic	ILE52	A	1.770
7	1TR7	-6.6	Hydrogen	ILE52	H	2.334
			Hydrogen	GLY79	H	2.630
			Hydrogen	ILE13	H	3.040
			Hydrogen	PRO104	H	1.832
			Electrostatic	ASP47	PAn	3.554
			Hydrophobic	ALA6	PA	5.286
8	1TR7	-6.4	Hydrogen	ILE52	H	2.996
			Hydrogen	TYR48	H	2.747
			Hydrophobic	ALA106	PA	5.445
9	1TR7	-6.7	Hydrogen	ASP47	H	1.875
			Hydrogen	SER39	C	3.716
			Hydrophobic	LYS101	A	4.696
			Hydrophobic	ILE13	A	4.050
			Hydrophobic	PHE1	A	4.553
			Hydrophobic	PRO102	PA	4.855
			Hydrophobic	ILE52	PA	5.458
10	1TR7	-6.9	Hydrogen	GLN133	H	2.358
			Electrostatic	PHE1	PCa	4.219
			Hydrophobic	TYR48	PPS	3.883
			Hydrophobic	ILE52	A	3.848
			Hydrophobic	TYR48	PA	4.781
			Hydrophobic	ILE13	PA	5.277
11	1TR7	-6.7	Hydrogen	TYR137	H	2.009
			Hydrogen	ASN46	H	2.322

	Hydrogen	THR40	H	2.212
	Hydrogen	GLN133	H	2.940
	Hydrogen	ASP47	PDH	3.069
	Hydrophobic	ILE13	PS	3.560
	Hydrophobic	ALA6	A	3.796
	Hydrophobic	ALA6	PA	5.423

H = Conventional hydrogen bond; C = Carbon hydrogen bond; A= Alkyl; PA = Pi-alkyl; PAn = Pi-Anion; PCa = Pi-cation; PS = Pi-sigma; PPS = Pi-Pi stacked; PDH = Pi-donor hydrogen bond.

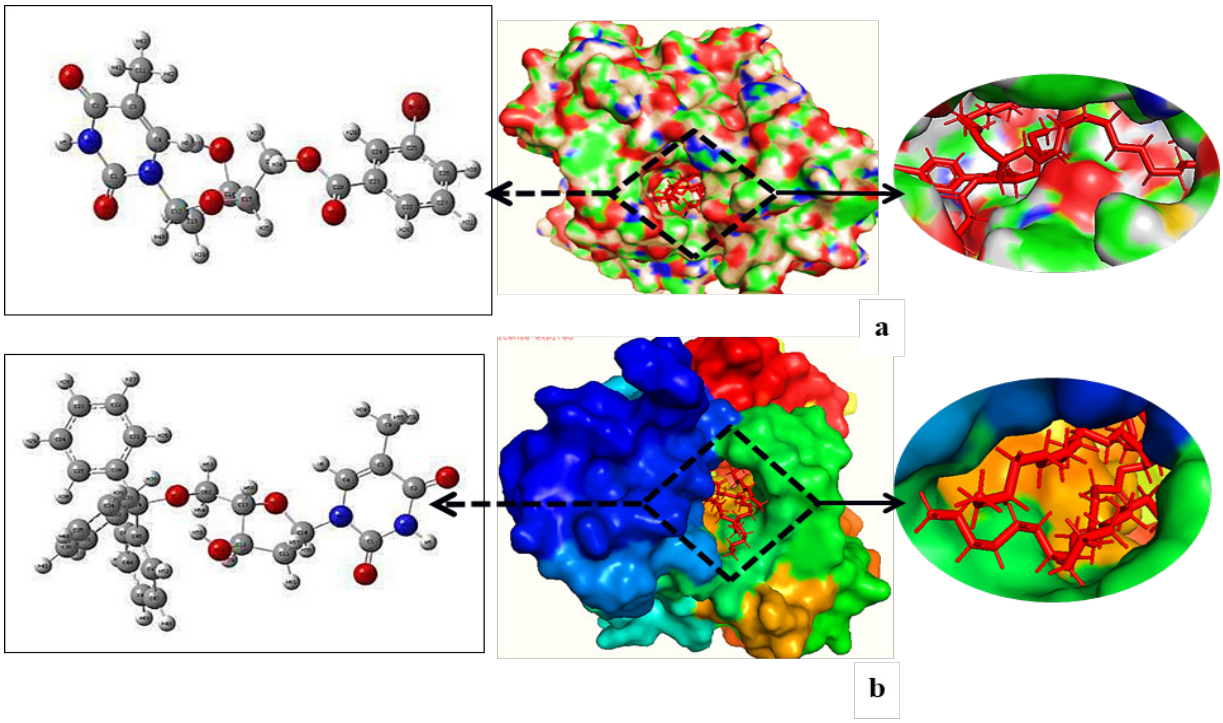

Figure 7. Docked conformation of derivative 10 at inhibition bounding site of 1TR7 (**a**) and docked conformation of derivative 11 at inhibition bounding site of 1TR7 (**b**).

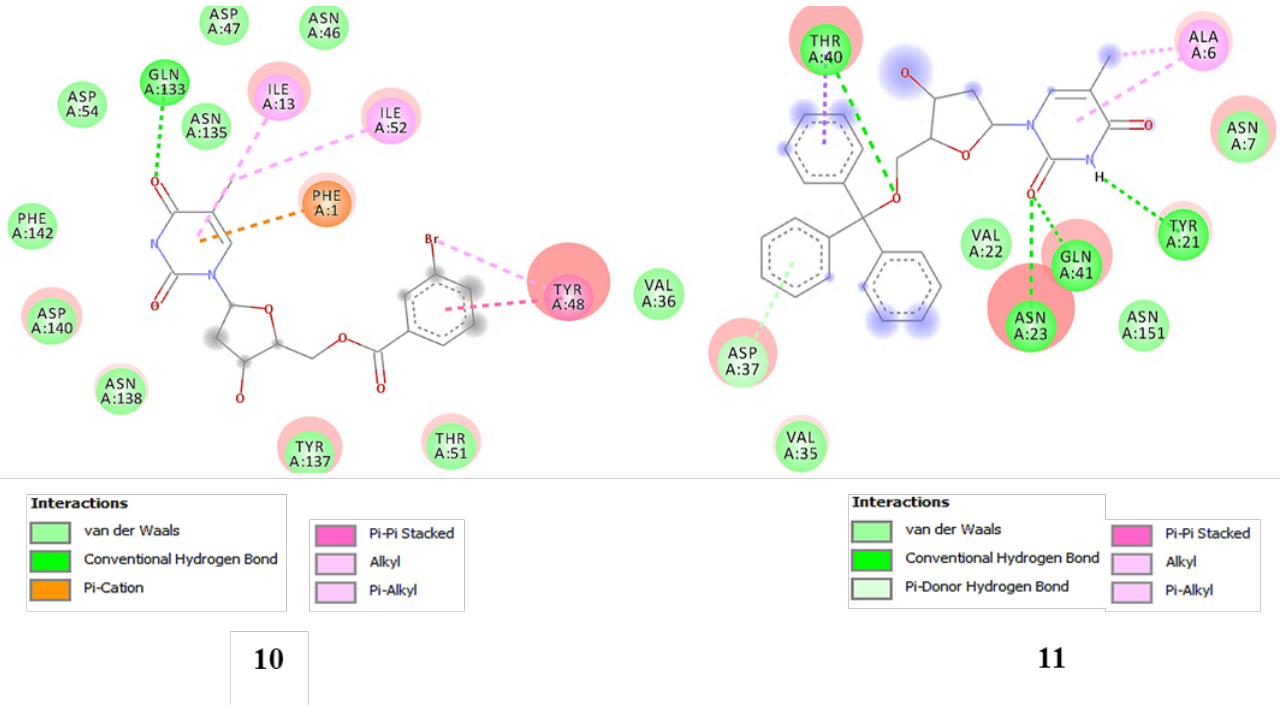

Figure 8. Non-bonding interactions of compounds 9 and 10 with the amino acid residues of 1TR7 generated by Discovery Studio.

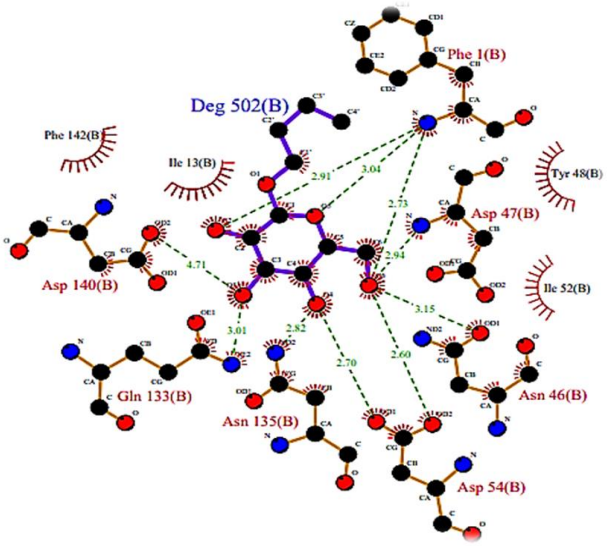

Figure 9. Two-dimensional LigPlot image of FimH complex generated by PDBsum.

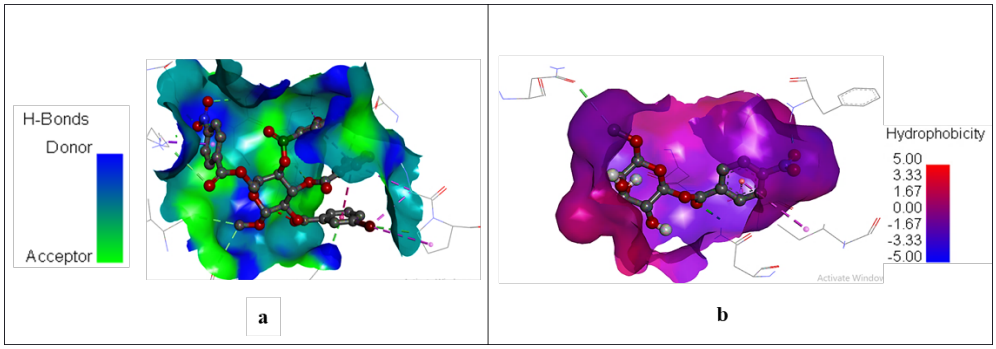

Figure 10. Hydrogen bond surface and hydrophobic surface of 1TR7 with compound 5 (**a**) and compound 9 (**b**).

Recent studies reported that the Tyr48 is considered as the principal component of the PPS, responsible for the accessibility of small molecules to the active site. Binding affinity and binding specialty were improved in the case of 2, 4, 5, 6, 7, and 11 due to significant hydrogen bonding. It was observed that modifications of the –OH group of thymidine 1 enhanced the π-π interactions with the residues of the active site while increasing their polarity resulted in the formation of hydrogen bonding interactions. The most prominent H-bonds were obtained for the derivative 5, formed with Asp54, Gln133, Asn46, Ile13, and Asn133. Hydrogen bonds executed a vital function in shaping the specificity of ligand binding with the receptor, drug design in chemical and biological processes, molecular recognition, and biological activity [55]. The hydrogen bond surface of derivative 5 and the hydrophobic surface of derivative 9 are consequently represented in Figure 10. We realize that the analyzed thymidine derivatives were bound within some of the catalytic binding sites such as isoleucines (Ile13 and Ile52), Tyr48, Tyr137, Asp46, Asp54, Asp140, Asn46, Asn135, Gln133, and Phe1 of the FimH, which is responsible for acute and recurrent bladder infections and chronic inflammatory bowel diseases such as Crohn's disease. Among all the molecules, the inhibition activity of the derivative 10 was found to be the highest (-6.7 kcal/mol). The results were summarized into a set of structural changes to be used in FimH-targeted inhibitor design: thymidine derivatives gave an improved affinity and inhibitory potential; because of their relative flexibility combined with a favorable interaction with isoleucine-52 located in the middle of the tyrosine gate.

Pharmacokinetic prediction and Lipinski's rule

In order to predict that the modified derivatives are potential drugs, we used the *in silico* pharmacokinetic parameters ADMET. The pkCSM online server [56] was employed to calculate *in silico* ADMET properties (Table 5). The absorbance value below 30% indicated poor absorbance; most of the compounds displayed a value above 60%, which revealed a good absorbance in the human intestine.

Table 5. *In silico* ADMET prediction of thymidine and its derivatives.

Entry	Absorption	Distribution			Metabolism					Excretion		Toxicity
	Intestinal absorption (human)	VDss (human)	BBB permeability	CNS permeability	Substrate		Inhibitor			Total Clearance		AMES toxicity
					CYP							
					2D6	3A4	1A2	2C19	2D6	3A4		
	Numeric (% Absorbed)	Numeric (Log L/kg)	Numeric (Log BB)	Numeric (Log PS)	Categorical (Yes/No)					Numeric (Log ml/min/kg)		Categorical (Yes/No)
1	60.686	0.395	-0.982	-2.649	No	Yes	Yes	Yes	No	Yes	0.729	No
2	61.061	0.409	-0.950	-3.646	No	Yes	No	Yes	No	Yes	1.446	No
3	61.802	0.405	-0.380	-3.634	No	Yes	Yes	Yes	No	Yes	1.454	No
4	62.236	0.494	0.334	-2.615	No	Yes	Yes	Yes	No	Yes	1.507	No
5	63.364	0.459	0.323	-2.919	No	Yes	Yes	Yes	No	Yes	1.585	No
6	65.540	0.439	0.310	-2.884	No	Yes	Yes	Yes	No	Yes	1.664	No
7	68.304	0.465	0.327	-2.837	No	Yes	No	Yes	No	Yes	1.357	No
8	69.892	0.506	0.385	-2813	No	Yes	Yes	Yes	No	Yes	1.388	No
9	69.418	0.402	0.274	-2.147	No	Yes	Yes	Yes	No	Yes	-0.109	No
10	69.227	0.409	0.305	-1.146	No	Yes	Yes	Yes	No	Yes	-0.071	No
11	89.906	0.525	0.920	-1.676	No	Yes	Yes	Yes	No	Yes	0.650	No

It is evident that the volume of distribution (VDss) was supposed to be high if the value was higher than 0.45. In addition, blood-brain barrier (BBB) and central nervous system (CNS) permeability had standard values (>0.3 to < -1 log BB, and > -2 to < -3 log PS), respectively. A given compound with a log BB < -1 is poorly distributed to the brain, while that with log BB >0.3 means a potential to cross BBB and with log PS > -2 is considered to penetrate the CNS, while with log PS < -3 it is difficult to move in the CNS [57]. It was observed that most of the compounds exhibited a significant potential to cross the barriers except derivatives 2, and 3. The enzymatic metabolism ensures the chemical biotransformation of a designed drug in the body, which plays a key role in the transformation of drug compounds. In the body, drugs produce several enzymatic metabolites which play a role in catalyzing the reaction with several drug concentrations [58]. It is essential to consider the metabolism of drugs, which may show several physicochemical and pharmacological parameters. The cytochrome P450 (CYP450) plays a major role in drug metabolism because of the major liver enzyme system involved in phase 1 metabolism. Some selective CYP genes of CYP1, CYP2, CYP3, and CYP4 families were found to be involved in drug metabolism, with CYP (1A2, 2C19, 2D6, and 3A4) causing the biotransformation of more than 90% of drugs undergoing phase I metabolism. Therefore, among these members, CYP3A4 is the most important inhibition in this study [59]. All designed derivatives were found to be the substrate and the inhibitor of CYP3A4. Clearance is a constant that indicates the relationship between drug concentration in the body and the rate of elimination of the drug. Therefore, all modified derivatives showed a somewhat high value but were still acceptable in the persistence of the drug in the body. Moreover, it is essential to test whether the calculated derivatives are non-toxic because this plays a critical role in the selection of drugs. All the derivatives we designed are non-toxic. Overall, derivatives 4–11 have better *in silico* pharmacokinetic properties.

Generally, drug-likeness is evaluated using Lipinski's rule of five [60]. As a matter of principle, an orally active drug should have no more than one interruption of the following conditions: (1) no more than five hydrogen bond donors, (2) no more than ten hydrogen bond acceptor, (3) molecular mass of less than 500 Da, (4) an octanol-water partition coefficient of not more than five, and (5) molar refractivity <140. If two or more of the guidelines are disrupted, reduced absorption can be estimated. All of the thymidine derivatives did not violate any of Lipinski's rule of five (Tables 6 and 7). However, topological polar surface area (TPSA) is a contributing factor for oral absorption and blood-brain barrier permeation capacity and the screened drug-likeness of a molecule should have TPSA between 20 and 130 Å^2. The SwissADME web tool prediction ravels that only derivative 11 violates this TPSA standard and all others ligands

are anticipated to be orally bioavailable. In addition, Pan-assay interference derivatives (PAINS) revealed no violation with these thymidine derivatives. PAINS are chemical compounds that often give false-positive results in high-throughput screens. PAINS tend to react nonspecifically with numerous biological targets rather than specifically affecting one desired target. The derivatives designed were evaluated for their synthetic accessibility, the synthetic accessibility values for all derivatives designed are about 3 to 5, therefore, they are easy to synthesize. In fine, the new compounds 2–4 and 9–11 respect all drug-likeness rules.

Table 6. Drug-likeness prediction of thymidine and its derivatives.

Entry	Molar Refractivity (Å)	Log $P_{o/w}$ (XLOGP3)	NRB	NHA	NHD	TPSA (Å²)	Csp3
1	58.070	-1.510	2	5	3	104.550	0.601
2	72.621	0.391	5	6	2	110.620	0.620
3	77.422	1.874	6	6	2	110.620	0.640
4	87.044	1.940	8	6	2	110.620	0.691
5	101.460	3.322	11	6	2	110.620	0.744
6	115.882	4.954	14	6	2	110.620	0.772
7	135.119	7.110	18	6	2	110.620	0.814
8	144.722	8.202	20	6	2	110.620	0.821
9	92.720	1.755	5	6	2	110.620	0.350
10	95.412	1.814	5	6	2	110.620	0.350
11	93.556	3.491	7	5	2	136.151	0.244

Table 7. Drug-likeness prediction of the thymidine esters basing on Lipinski, Muegge, Veber, Egan, Ghose, and their synthetic accessibility.

Entry	Lipinski	Muegge	Veber	Egan	Ghose	Synthetic accessibility	PAINS alert
1	Yes	Yes	Yes	Yes	Yes	3.641	0
2	Yes	Yes	Yes	Yes	Yes	3.960	0
3	Yes	Yes	Yes	Yes	Yes	4.064	0
4	Yes	Yes	Yes	Yes	Yes	4.281	0
5	Yes	Yes	No	Yes	Yes	4.625	0
6	Yes	Yes	No	Yes	Yes	4.972	0
7	Yes	No	Yes	Yes	No	5.454	0
8	Yes	No	No	Yes	No	5.701	0
9	Yes	Yes	Yes	Yes	Yes	4.025	0
10	Yes	Yes	Yes	Yes	Yes	4.106	0
11	Yes	Yes	Yes	Yes	Yes	5.040	0

Table 8. Predicted cytotoxic activity of the thymidine derivatives.

Entry	Cancer cell line prediction result			
	Blood (Leukemia)		Lung (Carcinoma)	
	Pa	Pi	Pa	Pi
1	0.640	0.007	0.569	0.024
2	-	-	0.502	0.016
3	0.515	0.013	0.570	0.024
4	0.505	0.014	0.568	0.024
5	0.505	0.014	0.568	0.024
6	0.505	0.014	0.568	0.024
7	0.505	0.014	0.568	0.024
8	0.505	0.014	0.568	0.024
9	-	-	0.503	0.048
10	-	-	-	-
11	0.522	0.013	0.523	0.039

Cytotoxic prediction

Web-based PASS was used to predict the cytotoxicity of modified thymidine derivatives. Childhood T acute lymphoblastic leukemia and non-small cell lung cancer -3 stages were predicted to suggest the maximum nontoxic bioactive drug molecule. It was evident from prediction Table 8 that thymidine derivatives 2–11 showed 0.50 < Pa < 0.52 for lymphoblastic leukemia, 0.50 < Pa < 0.56 lung cancer. There is a clear concept from the predicted data that these molecules have an equal potentiality to work against both of the cancer cells. Derivatives 3–8 exhibited the same types of activity (Pa ¼ 0.505) and (Pa ¼ 0.568) in spite of having a different aliphatic chain. Finally, derivative 11 which has a tri-phenyl ring revealed a comparatively higher activity (Pa ¼ 0.523) in both predictions. We hope to conduct such studies for a more drug-related validation of these promising thymidine derivatives.

CONCLUSION

In conclusion, several thymidine derivatives were successfully analyzed *in silico* for their antimicrobial, thermodynamic, molecular docking, pharmacokinetic, and drug-likeness properties. Quantum mechanical (QM) calculations of all the thymidine derivatives were performed to determine the thermodynamic parameters, atomic partial charge, and molecular electrostatic potential which revealed that insertion of aliphatic chains and halobenzoyl ring increased the stability of the thymidine derivatives. PASS prediction values of the thymidine derivatives 2–11 were Pa < 0.51 in antibacterial, Pa < 0.76 in antifungal, Pa < 0.77 in antiviral and Pa < 0.83 in anti-carcinogenic activity which revealed the antimicrobial potency of the modified derivatives. Molecular docking was employed to suggest the best antibacterials against *E. coli* (1TR7). Thymidine derivatives showed an interesting range of binding affinity -6.0 to -6.9 kcal/mol and strong interactions with at least one of the catalytic residues (Tyr48, Tyr137, Ile13, Ile52, Asp47, Asp54, Asp140, Asn46, Asn135, and Gln133) of the lectin FimH (1TR7). These derivatives showed several non-covalent interactions, such as hydrogen bonding, hydrophobic, and electrostatic interactions. These blind molecular docking analyses may provide a potential approach for the application of antibacterial drugs as expected inhibitors of *E. coli* protein lectin FimH. The docking validation process revealed that RMSD is in the standard range. Visual inspection exhibited very convincing results in the molecular docking validation process. In fine, these derivatives were analyzed for their pharmacokinetic properties which expressed that the combination of cytotoxic prediction, *in silico* ADMET prediction, and drug-likeness had shown promising results because the newly designed molecules have improved kinetic parameters and maintain all drug-likeness rules, as well as an interesting result in terms of biological activity. So, it could be concluded that most of the selected antibacterials showed promise and can be used to design effective antibacterial drugs against *E. coli* protein lectin FimH. More drug-likeness *in vitro* and *in vivo* studies such as nontoxic concentration towards healthy cells may be conducted in the near future.

Acknowledgement: *The authors are grateful to the Research and Publication Cell (Ref.: 6322/gobe/pari/proka/doptor/C.U./2018), University of Chittagong, Bangladesh for providing financial support to carry out this piece of research.*

REFERENCES

1. G. Niu, H. Tan, *Trends Microbiol*., **23** (2), 110 (2015).
2. K. L. Seley-Radtke, M. K. Yates, *Antiviral Res*., **154**, 66 (2018).
3. J. E. Polifka, J. M. Friedman, *Teratology*, **65** (5), 240 (2002).
4. M. Arifuzzaman, M. M. Islam, M. M. Rahman, M. A. Rahman, S. M. A. Kawsar, *Acta Pharm. Sci.*, **56** (4), 7 (2018).
5. T. S. Chowdhury, J. Ferdous, M. M. H. Misbah, M. Z. H. Bulbul, S. M. A. Kawsar, *J. Bangladesh Chem. Soc.*, **31** (2), 40 (2019).
6. A. Alam, M. A. Hosen, A. Hosen, Y. Fujii, Y. Ozeki, S. M. A. Kawsar, *J. Mexican Chem. Soc.*, **65**, 256 (2021).
7. L. P. Elwell, R. Ferone, G. A. Freeman, J. A. Fyfe, J. A. Hill, P. H. Ray, C. A. Richards, S. C. Singer, V. B. Knick, J. L. Rideout, *Antimicrob. Agents Chemother*., **31**(2), 274 (1987).
8. A. A. Krayevsky, K. A. Watanabe, Modified Nucleosides as Anti-AIDS Drugs: Current Status and Perspectives, Bioinform., Moscow, 1993.
9. S. Tabata, M. Yamamoto, H. Goto A. Hirayama, M. Ohishi, T. Kuramoto, A. Mitsuhashi, R. Ikeda, M. Haraguchi, K. Kawahara, Y. Shinsato, K. Minami, A. Saijo, M. Hanibuchi, Y. Nishioka, S. Sone, H. Esumi, M. Tomita, T. Soga, T. Furukawa, S.-I. Akiyama, *Cell Report*, **19** (7) 1313 (2017).
10. M. Z. H. Bulbul, T. S. Chowdhury, M. M. H. Misbah, J. Ferdous, S. Dey, I. Hasan, Y. Fujii, Y. Ozeki, S. M. A. Kawsar, *Pharmacia*, **68** (1), 23 (2021).
11. K. M. Rana, J. Ferdous, A. Hosen, S. M. A. Kawsar, *J. Sib. Fed. Univ. Chem.*, **13** (4), 465 (2020).

12. M. Z. H. Bulbul, M. A. Hosen, J. Ferdous, T. S. Chowdhury, M. M. H. Misbah, S. M. A. Kawsar, *Int. J. New Chem.,* **8** (1), 88 (2021).
13. J. Maowa, M. A. Hosen, A. Alam, K. M. Rana, Y. Fujii, Y. Ozeki, S. M. A. Kawsar, *Phys. Chem. Res*., **9**, 385 (2021).
14. M. I. Mirajul, M. Arifuzzaman, M. R. Monjur, M. R. Atiar, S. M. A. Kawsar, *Hacettepe J. Biol. Chem.*, **47**, 153 (2019).
15. S. R. Devi, S. Jesmin, M. Rahman, M. A. Manchur, Y. Fujii, R. A. Kanaly, Y. Ozeki, S. M. A. Kawsar, *Acta Pharm. Sci*., **57**, 47 (2019).
16. J. Maowa, A. Alam, K. M. Rana, S. Dey, A. Hosen, Y. Fujii, I. Hasan, Y. Ozeki, S. M. A. Kawsar, *Ovidius Univ. Annals Chem.,* **32**, 6 (2021).
17. K. M. Rana, J. Maowa, A. Alam, S. Dey, A. Hosen, I. Hasan, Y. Fujii, Y. Ozeki, S. M. A. Kawsar, *In Silico Pharmacol.,* **9**, 1 (2021).
18. S. M. A. Kawsar, M. A. Hosen, *Turk. Comput. Theor. Chem.,* **4** (2), 59 (2020).
19. A. L. Kau, D. A. Hunstad, S. J. Hultgren, *Curr. Opin. Microbiol*., **8** (1), 54 (2005).
20. F. A. Carvalho, N. Barnich, A. Sivignon, C. Darcha, C. H. Chan, C. P. Stanners, A. Darfeuille-Michaud, *J. Exp. Med*., **206** (10), 2179 (2009).
21. C. S. Hung, J. Bouckaert, D. Hung, J. Pinkner, C. Widberg, A. DeFusco, C. G. Auguste, R. Strouse, S. Langermann, G. Waksman, S. J. Hultgren, *Mol. Microbiol.*, **44** (4), 903 (2002).
22. A. Sivignon, X. Yan, D. Alvarez Dorta, R. Bonnet, J. Bouckaert, E. Fleury, J. Bernard, S. G. Gouin, A. Darfeuille-Michaud, N. Barnich, *mBio*., **6** (6), e01298 (2015).
23. N. Dreux, J. Denizot, M. Martinez-Medina, A. Mellmann, M. Billig, D. Kisiela, S. Chattopadhyay, E. Sokurenko, C. Neut, C. Gower-Rousseau, J-F. Colombel, R. Bonnet, A. Darfeuille-Michaud, N. Barnich, *PLoS Pathog*., **9** (1), e1003141 (2013).
24. D. Chatfield, J. Christopher, *Theoretical Chem. Acc*., **108**, 367 (2002).
25. S. M. A. Kawsar, M. A. Hosen, Y. Fujii, Y. Ozeki, *J. Comput. Chem. Mol. Model.,* **4** (4), 452 (2020).
26. F. Yasmin, M. R. Amin, M. A. Hosen, M. Z. H. Bulbul, S. Dey, S. M. A. Kawsar, *Cellulose Chem. Technol.,* **55**, 477 (2021).
27. S. M. A. Kawsar, A. Kumar, *J. Chilean Chem*. Soc., **66**, 5206 (2021).
28. F. Yasmin, M. R. Amin, M. A. Hosen, M. Z. H. Bulbul, S. Dey, S. M. A. Kawsar, *J. Sib. Fed. Univ. Chem.*, **14**, 171 (2021).
29. R. A. Gaussian, M. J. Frisch, G. W. Trucks, H. B. Schlegel, G. E. Scuseria, et al., Gaussian Inc., Wallingford, CT, 2009, https://gaussian.com/g09citation/.
30. A. D. Becke, *Phys. Rev., A*, **38**, 3098 (1988).
31. C. Lee, W. Yang, R. G. Parr, *Phys. Rev., B*, **37**, 785 (1988).
32. S. Kumaresan, V. Senthilkumar, A. Stephen, B. S. Balakumar, *World J. Pharmaceut. Res*., **4** (1) 1035 (2015).
33. H. M. Berman, J. Westbrook, Z. Feng, G. Gilliland, T. N. Bhat, H. Weissig, *Nucleic Acids Res*., **28**, 235 (2000).
34. W. L. Delano, The PyMOL molecular graphics system. De-Lano Scientific, San Carlos, CA, USA, 2002.
35. N. Guex, M. C. Peitsch, *Electrophoresis*, **18**, 2714 (1997).
36. S. Dallakyan, A. J. Olson, Small-molecule library screening by docking with Py Rx, in: J. E. Hempel, C. H. Williams, C. C. Hong (eds.), Chemical biology: methods and protocols. Springer, New York, USA, 2015, p. 243.
37. Version ADS 4.0, Accelrys, San Diego, USA, 2017.
38. K. Onodera, K. Satou, H. Hirota, *J. Chem. Inf. Model.,* **47**, 1609 (2007).
39. G. L. Warren, C. W. Andrews, A. M. Capelli, B. Clarke, J. LaLonde, M. H. Lambert, M. Lindvall, N. Nevins, S. F. Semus, S. Senger, G. Tedesco, I. Wall, J. M. Woolven, C.E. Peishoff, M. S. Head, *J. Med. Chem.,* **49** (20), 5912 (2006).
40. L. L. G. Ferreira, A. D. Andricopulo, *Drug Discov. Today*, **24**, 1157 (2019).
41. A. Daina, O. Michielin, V. Zoete, *Sci. Rep*., **7**, 1 (2017).
42. N. Cohen, S. W. Benson, *Chem. Rev*., **93**, 2419 (1993).
43. E. J. Lien, Z. R. Guo, R. L. Li, C. T. Su, *J. Pharm. Sci.,* **71**, 641 (1982).
44. M. M. Matin, P. Chakraborty, M. S. Alam, M. M. Islam, U. Hanee, *Carbohydr. Res*., **496**, 108130 (2020).
45. H. Heinz, U. W. Suter, *J. Phys. Chem*., *B*, **108**, 18341 (2004).
46. K. C. Gross, P. G. Seybold, C. M. Hadad, *Int. J. Quantum Chem*., **90**, 445 (2002).
47. R. S. Mulliken, *J. Chem. Phys*., **23**, 1833 (1955).
48. M. L. Amin, *Drug Target Insights*, **7**, 27 (2013).
49. P. Politzer, J. S. Murray, *Rev. Comput. Chem*., **2** 273 (1991).
50. P. Politzer, D. G. Truhlar (eds.), Chemical applications of atomic and molecular electrostatic potentials. Reactivity, structure, scattering, and energetics of organic, inorganic, and biological systems, Springer USA, 1981.
51. R. T. Kroemer, A. Vulpetti, J. J. McDonald, D. C. Rohrer, J. -Y. Trosset, F. Giordanetto, S. Cotesta, C. McMartin, M. Kihlen, P. F. W. Stouten, *J. Chem. Inf. Comput. Sci.,* **44** (3), 871 (2004).
52. G. Jones, P. Willett, R. C. Glen, A. R. Leach, R. Taylor, *J. Mol. Biol.,* **267** (3), 727 (1997).
53. M. Kontoyianni, L. M. McClellan, G. S. Sokol, *J. Med. Chem.,* **47** (3), 558 (2004).
54. R. Ghosh, A. Chakraborty, A. Biswas, S. Chowdhuri, *J. Biomol. Struct. Dyn*., 1 (2020).
55. J. Perlstein, *J. American Chem. Soc.,* **123**, 191 (2001).
56. D. E. V. Pires, T. L. Blundell, D. B. Ascher, *J. Med. Chem.,* **58**, 4066 (2015).
57. D. E. Clark, *Drug Discov. Today,* **8**, 927 (2003).

58. S. Kok-Yong, L. Lawrence, Drug distribution and drug elimination. Basic pharmacokinetic concepts, some clinical applications, InTechOpen, London, SW7 2QJ, UK, 2015.
59. M. M. Thapar, Pharmacokinetics and Dynamics of Atovaquone and Proguanil, Malarone®, Karolinska University Press, Stockholm, Sweden, 2004.
60. C. A. Lipinski, F. Lombardo, B. W. Dominy, P. J. Feeney, *Adv. Drug Deliv. Rev.,* **46**, 3 (2001).